Substituent dependence on the spin crossover behaviour of mononuclear Fe(II) complexes with asymmetric tridentate ligands

doi: 10.1039/C9DT00204A

Journal Name

ARTICLE

Substituent dependence on the spin crossover behaviour of mononuclear Fe(II) complexes with asymmetric tridentate ligands

Received 00th January 20xx,
Accepted 00th January 20xx

DOI: 10.1039/x0xx00000x

www.rsc.org/

Ryo Saiki,[a] Haruka Miyamoto,[a] Hajime Sagayama,[c] Reiji Kumai,[c] Graham N. Newton,[b] Takuya Shiga,*[a] and Hiroki Oshio*[a]

Three mononuclear iron(II) complexes of the formula $[Fe^{II}(H_2L^{1-3})_2](BF_4)_2 \cdot x(solv.)$ (H_2L^{1-3} = 2-[5-(R-phenyl)-1*H*-pyrazole-3-yl] 6-benzimidazole pyridine; H_2L^1: R = 4-methylphenyl, H_2L^2, R = 2,4,6-trimethylphenyl, H_2L^3, R = 2,3,4,5,6-pentamethylphenyl) (**1**, H_2L^1; **2**, H_2L^2; **3**, H_2L^3) with asymmetric tridentate ligands (H_2L^{1-3}) were synthesized and their structures and magnetic behaivor investigated. Significant structural distortions of the dihedral angles between phenyl and pyrazole groups were observed and found to depend on the nature of the substituent groups. Cryomagnetic studies reveal that **1** and **2** show gradual spin crossover behavior, while **3** remains in the high spin state between 1.8 and 300 K.

Introduction

Bistable molecules attract significant interest due to their potential applications as components in molecular electronic and nanoscale devices.[1] Spin crossover (SCO) molecules are one such class of bistable material that lend themselves to potential molecular switching applications.[2] SCO behaviour can be tuned by modifying ligand field strength, complex nuclearity and intermolecular interactions. Many systematic studies on the SCO behaviour of molecular species have shown dependence of the bistability on anions, guest molecules, solvent molecules and substituent groups.[3] Anions affect the crystal packing and intermolecular electrostatic interactions, while solvent molecules can interact with spin crossover complexes through hydrogen bonds or CH-π interactions, resulting in perturbation of the electronic states of SCO-active iron complexes. Matsumoto et al. reported a series of two-dimensional SCO complexes, $[Fe^{II}H_3L^{Me}][Fe^{II}L^{Me}]X$ (H_3L^{Me} = tris-[2-(((2-methylimidazol-4-yl)methylidene)aminoethyl)amine), X^- = ClO_4^-, BF_4^-, PF_6^-, AsF_6^-, SbF_6^-), which show different SCO behaviour depending on the nature of the interlayer elastic interactions mediated by the anions.[4] The influence of counter ions and solvent molecules in cobalt SCO systems has been discussed in detail by Real et al.[5] However, the origin of the effects on the SCO behaviour mediated by anion and solvent molecules can be difficult to precisely define due to the complex nature of supramolecular systems. In contrast, ligand substituent groups directly affect the electon-donating nature of the ligand, and the ligand field strength can be controlled based on precise molecular design. For example, tridentate 2,6-bis(pyrazol-1-yl)pyridine (bpp) ligands can be readily modified, and the nature of the substituent effect on the SCO properties of their complexes with iron is well understood,[6] and can be predicted by Hammett's rule.[7] Distinct differences in the SCO properties of $[Fe(bpp)]^{2+}$ analogues with different substitution groups were observed in solid and solution states.[8] Substituent groups also exert a secondary influence on complex SCO behaviour via their effect on complex topology and supramolecular packing structure. For example, $[Fe^{II}(qsal\text{-}X)_2]$ (qsal-X = 5-X-*N*-(8-quinolyl)salicylaldimines), X = F, Cl, Br, I) complexes exhibit different SCO behaviour, dependent on the nature of the supramolecular interactions of their halogen substituents.[9] In order to obtain fine-tuned SCO systems, systematic studies on substituent effects on complex structure and magnetic properties remain a key approach. We recently developed a mononuclear Fe(II) spin crossover system with asymmetric tridentate ligands H_2L (H_2L = 2-[5-(phenyl)-1*H*-pyrazole-3-yl] 6-benzimidazole pyridine), which shows spin transition around 260 K and found that the electronic state of the system could be effectively tuned by deprotonation of the pyrazole or benzimidazole moieties.[10]

In this work, new asymmetric tridentate ligands H_2L^{1-3} (H_2L^{1-3} = 2-[5-(R-phenyl)-1*H*-pyrazole-3-yl] 6-benzimidazole pyridine; H_2L^1: R = 4-methylphenyl, H_2L^2: R = 2,4,6-trimethylphenyl, H_2L^3: R = 2,3,4,5,6-pentamethylphenyl, Scheme 1) were designed as supports for SCO materials. Three bis-chelate type iron complexes, $[Fe^{II}(H_2L^{1-3})_2](BF_4)_2$ (**1**, H_2L^1; **2**, H_2L^2; **3**, H_2L^3), were synthesized, and their structures and magnetic properties were investigated.

[a] Graduate School of Pure and Applied Sciences, University of Tsukuba, Tennodai 1-1-1, Tsukuba, Ibaraki 305-8571, Japan.
[b] GSK Carbon Neutral Laboratories for Sustainable Chemistry, The University of Nottingham, Nottingham NG7 2TU, U.K.
[c] Photon Factory and Condensed Matter Research Center, Institute of Materials Structure Science, High Energy Accelerator Research Organization (KEK), Oho 1-1, Tsukuba, Ibaraki 305-0801, Japan.

Electronic Supplementary Information (ESI) available: [molecular structure of **1'** - **3'**, Mössbauer spectra of **1**, and LIESST behaviour of **1**]. CCDC 1889870-1889875 for **1'** – **3'**, respectively. For ESI and crystallographic data in CIF or other electronic format see DOI: 10.1039/x0xx00000x

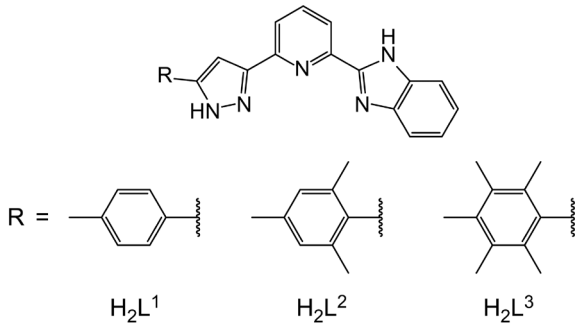

Scheme 1. Three asymmetric tridentate ligands L^1 - L^3.

Experimental

Materials

Unless otherwise stated, all starting materials and solvents were reagent grade and were purchased from Wako or Tokyo Chemical Industry Co. Ltd. and used without further purification.

Synthesis of $[Fe^{II}(H_2L^1)_2](BF_4)_2{\cdot}0.5(i\text{-}Pr_2O){\cdot}2(H_2O){\cdot}2(CH_3OH)$ (1). Methanol solution (5 mL) of $Fe(BF_4)_2{\cdot}6H_2O$ (30.0 mg, 0.09 mmol) was added to a solution of H_2L^1 (63.2 mg, 0.18 mmol) in methanol (10 mL). The resulting red solution was filtered and allowed to diffuse with *i*-Pr_2O. After a few days, red plates of $[Fe^{II}(H_2L^1)_2](BF_4)_2{\cdot}(i\text{-}Pr_2O){\cdot}2(CH_3OH)$ (**1'**) had formed. The crystals were collected by suction and air-dried, affording $[Fe^{II}(H_2L^1)_2](BF_4)_2{\cdot}0.5(i\text{-}Pr_2O){\cdot}2(H_2O){\cdot}2(CH_3OH)$ (**1**). Yield 55.9 mg (66.4 %). Elemental analysis Anal. (calc.) for $C_{49}H_{53}N_{10}O_{4.6}B_2F_8Fe_1$: C, 54.41 (54.32); H, 4.76 (4.93); N, 13.18 (12.93) %. IR (KBr): 3277.1 (s, $\nu_{N\text{-}H}$), 1084 (s, $\nu_{B\text{-}F}$) cm^{-1}.

Synthesis of $[Fe^{II}(H_2L^2)_2](BF_4)_2{\cdot}0.5(AcOEt){\cdot}0.5(H_2O){\cdot}1.5(CH_3OH)$ (2). Methanol solution (5 mL) of $Fe(BF_4)_2{\cdot}6H_2O$ (34 mg, 0.10 mmol) was added to a solution of H_2L^2 (75.8 mg, 0.20 mmol) in methanol (10 mL). The resulting red solution was filtered and allowed to diffuse with AcOEt. After a few days, red plates of $[Fe^{II}(H_2L^2)_2](BF_4)_2{\cdot}(AcOEt){\cdot}1.5(CH_3OH)$ (**2'**) were obtained. The crystals were collected by suction and air-dried, affording $[Fe^{II}(H_2L^2)_2](BF_4)_2{\cdot}0.5(AcOEt){\cdot}0.5(H_2O){\cdot}1.5(CH_3OH)$ (**2**). Yield 55.4 mg (56.1 %). Elemental analysis Anal. (calc.) for $C_{49.5}H_{49}N_{10}O_2B_2F_8Fe_1$: C, 56.51 (56.87); H, 5.01 (4.72); N, 13.30 (13.40) %. IR (KBr): 3280.9 (s, $\nu_{N\text{-}H}$), 1051.2 (s, $\nu_{B\text{-}F}$) cm^{-1}.

Synthesis of $[Fe^{II}(H_2L^3)_2](BF_4)_2{\cdot}2.5(H_2O){\cdot}(i\text{-}Pr_2O)$ (3). Methanol solution (5 mL) of $Fe(BF_4)_2{\cdot}6H_2O$ (34 mg, 0.10 mmol) was added to a solution of H_2L^3 (1.0 mg, 0.20 mmol) in methanol (10 mL). The resulting red solution was filtered and allowed to diffuse with *i*-Pr_2O. After a few days, red plates of $[Fe^{II}(H_2L^3)_2](BF_4)_2{\cdot}2(i\text{-}Pr_2O)$ (**3'**) were obtained. The crystals were collected by suction and air-dried, affording $[Fe^{II}(H_2L^3)_2](BF_4)_2{\cdot}2.5(H_2O){\cdot}(i\text{-}Pr_2O)$ **(3).** Yield 33.4 mg (32 %). Elemental analysis Anal. (calc.) for $C_{52}H_{55}N_{10}O_{2.5}B_2F_8Fe_1$: C, 57.51 (57.32); H, 5.20 (5.09); N, 12.55 (12.86) %. IR (KBr): 3280.8 (s, $\nu_{N\text{-}H}$), 1057.0 (s, $\nu_{B\text{-}F}$) cm^{-1}.

Physical measurements

Physical measurements were performed using air-dried samples **1** – **3**, except for the single crystal X-ray measurements, in which fresh samples **1'** – **3'** were used. Infrared (IR) spectra were recorded (400 - 4000 cm^{-1}) on a SHIMADZU IRAffinity-1 spectrometer using KBr pellets. Direct current magnetic susceptibility measurements of polycrystalline samples for **1** - **3** were measured in the temperature range of 1.8 – 300 K with a Quantum Design MPMS-5XL SQUID magnetometer under an applied magnetic field of 500 Oe or 1 T. Data were corrected for the diamagnetic contribution calculated from Pascal's constants including the contribution of the sample holder.

Data collections for single crystal X-ray diffraction for **1'** – **3'** were performed on a Bruker SMART APEX II for all complexes, with a CCD area detector with graphite monochromated Mo-K_α (λ = 0.71073 Å) radiation. All structures were solved by direct methods and refined by full-matrix least-squares methods based on F^2 using the SHELXL software. Non-hydrogen atoms were refined anisotropically. All hydrogen atoms were positioned geometrically and refined with isotropic displacement parameters according to the riding model. All geometrical calculations were performed using the SHELXL software. X-ray diffraction experiments at 20 K for complex **1'** after light irradiation using green laser (532 nm) were performed by using the synchrotron radiation source (λ = 1.0 Å) at Photon Factory BL-8A in High Energy Accelerator Research Organization (KEK), Japan. The diffraction data were collected on the Imaging plate system (Rigaku). The structures were solved by direct methods and refined by full-matrix least-square techniques on F^2 using SHELXTL. The A-level alerts in checkcif for the data of Complex **1'** at KEK are due to the experiments using the KEK synchrotron. The detector is cylindrical and therefore has a huge diffraction angle range but can only rotate the crystal along one axis. Therefore, all possible reflections cannot be obtained. The A-level alert in checkcif for **2'** is due to the disorder of the BF_4^- anion.

Variable-temperature Mössbauer experiments were carried out using a ^{57}Co/Rh source in a constant acceleration transmission spectrometer (Topologic Systems) equipped with an Iwatani HE05/CW404 Cryostat. The spectra were recorded in the temperature range of 20–300 K. The spectrometer was calibrated using standard α-Fe foil.

Syntheses

The mononuclear bis-chelate iron(II) complexes (**1**-**3**) with asymmetric tridentate ligands $H_2L^{1\text{-}3}$ was synthesized. All complexes were synthesized in methanolic solution, but crystallizations for single crystal X-ray crystallography were performed using different antisolvents. Fresh single crystals tend to lose lattice solvent to the air. Therefore, physical measurements were performed using air-dried samples.

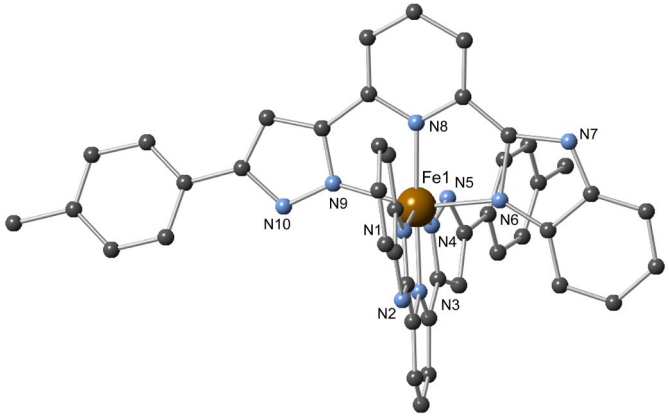

Fig. 1. Molecular structure of **1'**. Lattice solvents and anions have been omitted for clarity. Colour code: C, grey; N, light blue; Fe(II), brown. One benzimidazole moiety of the disordered ligand has been omitted for clarity.

Crystal structure of 1'

Complex **1'** crystallizes in the monoclinic space group *C*2/c (Figure 1). The cationic part of the complex consists of two H_2L^1 ligands and one Fe(II) ion, forming a bis-chelate type mononuclear structure. The Fe(II) ion exists in an octahedral coordination environment, coordinated by six nitrogen atoms from two H_2L^1 ligands. At 100 K, the coordinated benzimidazole group was solved in two positions, the occupancies of which were equal (Figure S1). The average Fe-N distances are 2.088 Å and 2.104 Å, and the Σ values are 105.8° and 134.4° for low and high spin parts, respectively. From the data collected at 20 K with the synchrotron X-ray source, a similarly disordered structure was determined. The average Fe-N distances are 2.063 Å and 2.097 Å, and the Σ values are 110.6° and 138.3° for low and high spin parts, respectively. The average dihedral angle between the pyrazole and trimethylphenyl moieties is 12.30° (Figure 2a) at 100 K.

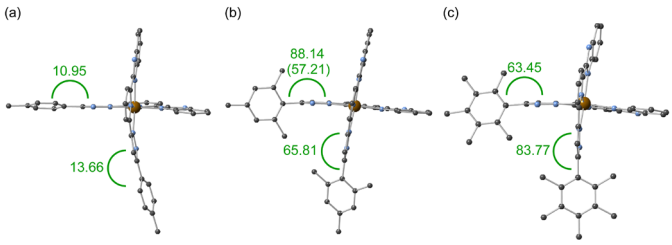

Fig. 2. Dihedral angles between pyrazole and phenyl groups of (a) **1'**, (b) **2'** and (c) **3'** at 100 K. For **2'**, one orientation of the disordered trimethylphenyl group was shown. Angles were indicated green letter, and the value of disordered group was shown in parentheses.

In this structure, hydrogen bonded interactions were observed between the pyrazole and benzimidazole moieties. Two pyrazole N atoms of the iron complex interact with BF_4^- anions, forming a one-dimensional chain network along the *b* axis (Figure 3). Two benzimidazole N atoms interact with methanol molecules. There are π stacking interactions between pairs of 4-methylphenyl and benzimidazole groups, resulting a tetramer of iron complexes.

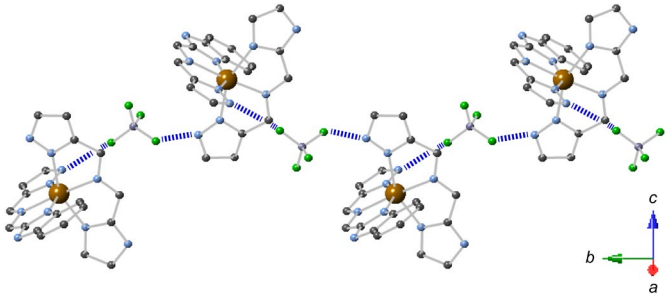

Fig. 3. One-dimensional chain network structure of **1'**. Carbon atoms of phenyl and pyridyl rings were omitted for clarity. Lattice solvents and non-interacting BF_4^- anions have been omitted. Colour code: C, grey; N, light blue; Fe(II), brown.

Crystal structure of 2'

Complex **2'** crystallizes in the triclinic space group $P\bar{1}$ (Figure S2). The structure of **2'** is similar to **1'**, but the solvent molecules and intermolecular interactions were different. At 100 K, the average Fe-N distance is 2.129 Å, and the Σ value is 136.5°, indicating a mixture of low and high spin complexes. The lattice contains disordered trimethyl phenyl groups and BF_4^- anions. The average dihedral angle between the pyrazole and trimethylphenyl moieties is 70.39° (Figure 2b). Hydrogen bonded interactions are operative between two pyrazole groups and methanol molecules and two benzimidazole groups and BF_4^- anions respectively, forming a one-dimensional chain structure along the *b* axis (Figure 4). There are π stacking interactions between benzimidazole moieties, forming a dimer of iron complexes.

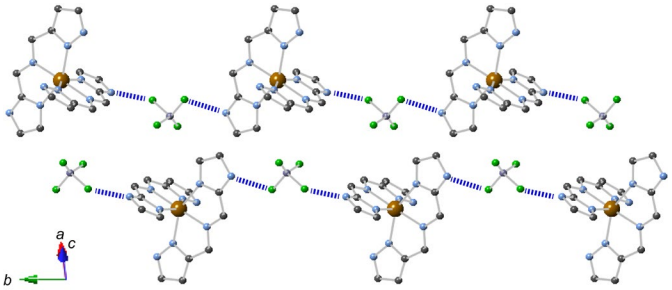

Fig. 4. One-dimensional chain network structure of **2'**. Carbon atoms of the phenyl and pyridyl rings were omitted for clarity. Lattice solvents and non-interacting BF_4^- anions have been omitted. Colour code: C, grey; N, light blue; Fe(II), brown.

Crystal structure of 3'

Complex **3'** crystallizes in the monoclinic space group $P2_1/n$ (Figure S3). The structure of **3'** is also similar to that of **1'**, but again, the solvent molecules and interactions with counter anions are different. The Fe(II) ion exists in an octahedral coordination environment, coordinated by six nitrogen atoms from two H_2L^3 ligands. At 100 K, the average Fe-N distance is 2.178 Å, and the Σ value is 142.3°, indicative of an iron(II) ion in the high spin state. The average dihedral angle between pyrazole and trimethylphenyl moieties is 73.61° (Figure 2c). Disordered BF_4^- anions are present in the lattice. One pyrazole moiety interacts with a solvent $^i Pr_2O$ molecule, while the other pyrazole group interacts with a BF_4^- anion. Two benzimidazole groups interact with BF_4^- anions. In the lattice, BF_4^- anions link

mononuclear iron moieties, forming a one-dimensional network structure (Figure 5). There are two kinds of π stacking interactions; one between pentamethylphenyl and benzimidazole groups, and the other between two benzimidazole groups.

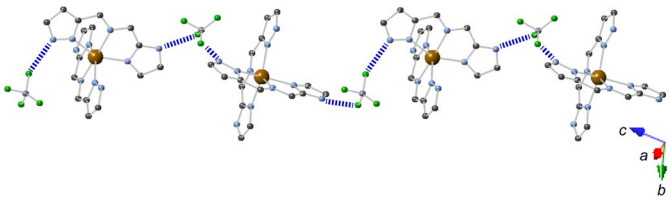

Fig. 5. One-dimensional chain network structure of **3'**. Carbon atoms of phenyl and pyridyl rings were omitted for clarity. Lattice solvents and non-interacting BF_4^- anions have been omitted. Colour code: C, grey; N, light blue; Fe(II), brown.

Distinct distortions of the dihedral angles between the pyrazole and phenyl groups were observed depending on the differences between the substituent groups. The trimethyl and pentamethyl groups are likely to cause significant steric hindrance of the neighbouring pyrazole moieties, resulting in large dihedral angles. This twisting of the molecules affects the intermolecular interactions such as π stacking and hydrogen bonds.

Magnetic properties

The magnetic susceptibilities of **1** - **3** were studied by SQUID magnetometry. The $\chi_m T$ vs. T plots for all complexes are shown in Figure 6. Complexes **1** and **2** show gradual SCO behaviour, while complex **3** has a high spin state (S = 2) in the whole temperature range. The $\chi_m T$ values for **1** and **2** at room temperature are 3.11 and 3.37 emu mol^{-1} K, values consistent with magnetically isolated high-spin Fe(II) ions (S = 2). Spin crossover temperatures for **1** and **2** were determined by maxima on the dχ/dT plots, affording 200 K and 250 K, respectively. Below 100 K, the $\chi_m T$ values for **1** and **2** were almost constant (1.46 and 1.59 emu mol^{-1} K, respectively). The paramagnetic state indicates partial spin transition of the iron ions, in agreement with the structural data discussed above. Complexes **1** – **3** exhibit different magnetic behaviour originating from the steric and packing effects of the ligands. We also note that the densities of the crystals are 1.347, 1.385, and 1.324 g cm^{-3} for complexes **1'**, **2'** and **3'** respectively. One can also speculate that this may influence the magnetic behaviour and that the lower density exhibited by **3'** may stabilise a high spin state in the lower temperature region. A detailed consideration of packing effects will require estimation of precise thermodynamic parameters and DFT calculations.[11]

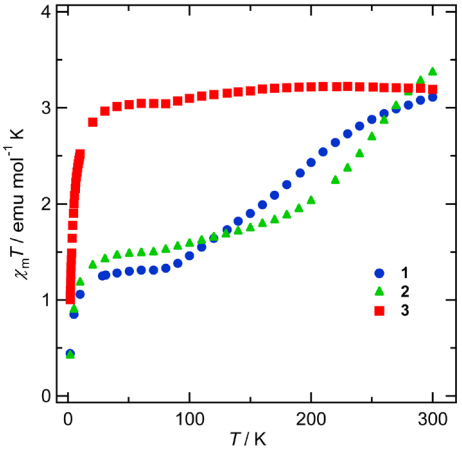

Fig. 6. Magnetic properties of **1** (●), **2** (▲), and **3** (▪).

In order to elucidate this partial spin transition, Mössbauer spectra were measured for complex **1** at 20 K and 300 K (Figure S7). At 20 K, the data can be analysed as a mixture of high- and low spin iron(II) species. On the other hand, the data collected at 300 K reveals only high spin iron(II) species. These facts indicate the occurrence of partial spin crossover in **1**. The obtained fitting parameters for Fe(II) high- or low-spin species are reasonable values for low symmetry SCO complexes (Tables S3 and S4).[12] Structural analysis of **1'** at 270 K was also performed, and confirmed that the iron ion has a high spin state based on coordination bond length (2.173 Å) and Σ value (140.0°). These data are consistent with partial spin crossover behaviour.

LIESST experiments were conducted on complex **1**, and the magnetic data is shown in Figure S8. An increase in $\chi_m T$ values was observed after light irradiation with a green. Structural analyses after light irradiation were also performed at the KEK synchrotron and the high spin spin state of iron(II) ion was confirmed based on average coordination bond lengths (2.127 Å) and Σ values (129.1°).

Conclusions

Three iron(II) complexes of the general formula $[Fe^{II}(H_2L^{1-3})_2](BF_4)_2 \cdot x(solv.)$, with different substituent groups, were synthesized and their electronic states were investigated. Complexes **1** and **2** show spin crossover behaviour, while **3** has a high-spin state in the temperature range of 1.8 - 300 K. Asymmetric ligands with benzimidazole and pyrazole coordination moieties are found to provide iron(II) centres with ligand field strengths of the right order to allow spin crossover phenomena. The substituent groups affect the supramolecular packing of the molecular species. These structural perturbations are passed on to the coordination geometries of the iron ions, significantly influencing the spin states of the complexes. This insight into the design of modified asymmetric mononuclear SCO complexes will aid in the future fine design of bistable molecular systems.

Conflicts of interest

There are no conflicts to declare.

Acknowledgements

This work was supported by a Grant-in-Aid for Scientific Research (C) (no. 17K05800) and Grant-in-Aid for Scientific Research on Innovative Areas 'Coordination Asymmetry' (no. JP16H06523) from the Japan Society for the Promotion of Science (JSPS). This work was performed under the approval of the Photon Factory Program Advisory Committee (Proposal No. 2018G102).

Notes and references

1 Application of Bistable molecules toward electronics and nanodevices: W.R. Browne and B.L. Fringa, *Chimia*, 2010, **64**, 398-403; O. Sato, J. Tao and Y.-Z. Zhang, *Angew. Chem. Int. Ed.*, 2007, **46**, 2152-2187; T. Tezgerevska, K.G. Alley and C. Boskovic, *Coord. Chem. Rev.*, 2014, **268**, 23-40; S. Sanvito, *Chem. Soc. Rev.*, 2011, **40**, 3336-3355; L. Bogani and W. Wernsdorfer, *Nat. Mat.*, 2008, **7**, 179-186; A.C. Fahrenbach, S.C. Warren, J.T. Incorvati, A.-J. Avestro, J.C. Barnes, J.F. Stoddart and B.A. Grzybowski, *Adv. Mat.*, 2013, **25**, 331-348; E. Ruiz, *Phys. Chem. Chem. Phys.*, 2014, **16**, 14-22.

2 SCO review: P. Gütlich and H.A. Goodwin Eds. *Spin Crossover in Transition Metal Compounds I, II, and III*, Springer-Verlag, Berlin, Germany, 2004; A. Bousseksou, G. Molnár, L. Salmon and W. Nicolazzi, *Chem. Soc. Rev.*, 2011, **40**, 3313-3335; M.A. Halcrow, *Chem. Soc. Rev.*, 2011, **40**, 4119-4142; J. Olguín and S. Brooker, *Coord. Chem. Rev.*, 2011, **255**, 203-240; P. Gütlich, Y. Garcia and H.A. Goodwin, *Chem. Soc. Rev.*, 2000, **29**, 419-427; D.J. Harding, P. Harding and W. Phonsri, *Coord. Chem. Rev.*, 2016, **313**, 38-61; P. Guionneau, *Dalton Trans.*, 2014, **43**, 382-393; P. Gamez, J.S. Costa, M. Quesada and G. Aromí, *Dalton Trans.*, 2009, **38**, 7845-7853.

3 SCO control by anions, guest molecules, solvents, and substituent groups: M. Yamada, H. Hagiwara, H. Torigoe, N. Matsumoto, M. Kojima, F. Dahan, J.P. Tuchagues, N. Re and S. Iijima, *Chem. Eur. J.*, 2006, **12**, 4536-4549; L.J.K. Cook, R. Kulmaczewski, R. Mohammed, S. Dudley, S.A. Barrett, M.A. Little, R.J. Deeth and M.A. Halcrow, *Angew. Chem. Int. Ed.*, 2016, **55**, 4327-4331; R.G. Miller and S. Brooker, *Chem. Sci.*, 2016, **7**, 2501-2505; S.A. Barrett and M.A. Halcrow, *RSC Adv.*, 2014, **4**, 11240; M. Fumanal, F. Jiménez-Grávalos, J. Ribas-Arino and S. Vela, *Inorg. Chem.*, 2017, **56**, 4474-4483; E. Coronado, M.Giménez-Marqués, G.M. Espallargas, F. Rey and I.J. Vitórica-Yrezábal, *J. Am. Chem. Soc.*, 2013, **135**, 15986-15989; G.J. Halder, C.J. Kepert, B. Moubaraki, K.S. Murray and J.D. Cashion, *Science*, 2002, **298**, 1762-1765; M.B. Bushuev, D.P. Pishchur, V.A. Logvinenko, Y.V. Gatilov, I.V. Korolkov, I.K. Shundrina, E.B. Nikolaenkova and V.P. Krivopalov, *Dalton Trans.*, 2016, **45**, 107-120.

4 M. Yamada, M. Ooidemizu, Y. Ikuta, S. Osa, N. Matsumoto, S. Iijima, M. Kojima, F. Dahan and J.-P. Tuchagues, *Inorg. Chem.*, 2003, **42**, 8406-8416.

5 A. Galet, A.B. Gaspar, M.C. Munoz, J.A. Real, *Inorg. Chem.*, 2006, **45**,4413-4422

6 SCO complex with bpp ligand: L.J.K. Cook, R. Mohammed, G. Sherborne, T.D. Roberts, S. Alvarez and M.A. Halcrow, *Coord. Chem. Rev.*, 2015, **289-290**, 2-12; M.A. Halcrow, *Coord. Chem. Rev.*, 2009, **253**, 2493-2514; G.A. Craig, O. Roubeau and G. Aromi, *Coord. Chem. Rev.*, 2014, **269**, 13-31; R.J. Deeth, M.A. Halcrow, L.J.K. Cook and P.R. Raithby, *Chem. Eur. J.*, 2018, **24**, 5204-5212; T.D. Roberts, F. Tuna, T.L. Malkin, C.A. Kilner and M.A. Halcrow, *Chem. Sci.*, 2012, **3**, 349-354; M.A. Halcrow, *New J. Chem.*, 2014, **38**, 1868-1882.

7 A. Kimura and T. Ishida, *Inorganics*, 2017, **5**, 52.

8 L.J.K. Cook, R.Kulmaczewski, R. Mohammed, S. Dudley, S.A. Barrett, M.A. Little, R.J. Deeth and M.A. Halcrow, *Angew. Chem. Int. Ed.*, 2016, **55**, 4327-4331.

9 W. Phonsri, D.S. Macedo, K.R. Vignesh, G. Rajaraman, C.G. Davies, G.N.L. Jameson, B. Moubaraki, J.S. Ward, P.E. Kruger, G. Chastanet and K.S. Murray, *Chem. Eur. J.*, 2017, **23**, 7052-7065.

10 Unpublilshed results (Submitted to *Angew. Chem. Int. Ed.*), T. Shiga, R. Saiki, L. Akiyama, R. Kumai, D. Natke, F. Renz, J.M. Cameron, G.N. Newton and H. Oshio

11 M.B. Bushuev, D.P. Pishchur, V.A. logvinenko, Y.V. Gatilov, I.V. Korolkov, I.K. Shundrina, E.B. Nikolaenkova and V.P. Krivopalov, *Dalton Trans.*, 2016, **45**, 107-120; S.Vela, J.J. Novoa and J. Ribas-Arino, *Phys. Chem. Chem. Phys.*, 2014, **16**, 27012-27024; M. Kepenekian, B.L. Guennic and V. Robert, *J. Am. Chem. Soc.*, 2009, **131**, 11498-11502; S. Vela and H. Paulsen, *Dalton Trans.*, Advance Article doi: 10.1039/C8DT04394A.

12 H. Naggert, J. Rundnik, L. Kipgen, M. Bernien, F. Nickel, L.M. Arruda, W. Kuch, C. Näther and F. Tuczek, *J. Mater. Chem. C* 2015, **3**, 7870-7877; M. Steinert, B. Schneider, S. Dechert, S. Demeshko and F. Meyer, *Inorg. Chem.*, 2016, **55**, 2363-2373; A.B. Gaspar, V. Ksenofontov, S. Reiman, P. Gutlich, A.L. Thompson, A.E. Goeta, M.C. Muñoz and J.A. Real, *Chem. Eur. J.*, 2006, **12**, 9289-9298; D.J. Harding, D. Sertphon, P. Harding, K.S. Murray, B. Moubaraki, J.D. Cashion and H. Adams, *Chem. Eur. J.*, 2013, **19**, 1082-1090; D.L. Reger, J.R. Gardinier, M.D. Smith, A.M. Shahin, G.J. Long, L. Rebbouh and F. Grandjean, *Inorg. Chem.*, 2005, **44**, 1852-1866; O. Iasco, E. Rivière, R. Guillot, M.B.-L. Cointe, J.-F. Meunier, A. Bousseksou and M.-L. Boillot, Inorg. Chem., 2015, 54, 1791-1799; J.G. Park, I.-R. Jeon and T.D. Harris, *Inorg. Chem.*, 2015, **54**, 359-369; H.V. Phan, P. Chakraborty, M. Chen, Y.M. Calm, K. Kovnir, L.K. Keniley, Jr., J.M. Hoyt, E.S. Knowles, C. Besnard, M.W. Meisel, A. Hauser, C. Achim and M. Shatruk, *Chem. Eur. J.*, 2012, **18**, 15805-15815; B. Schneider, S. Demeshko, S. Neudeck, S. Dechert and F. Meyer, *Inorg. Chem.*, 2013, **52**, 13230-13237; A.Y. Verat, N. Ould-Moussa, E. Jeanneau, B.L. Guennic, A. Bousseksou, S.A. Borshch and G.S. Matouzenko, *Chem. Eur. J.*, 2009, **15**, 10070-10082.